Numerical Modeling of Magnetic Field Deformation as Related to Susceptibility Measured with an MR System

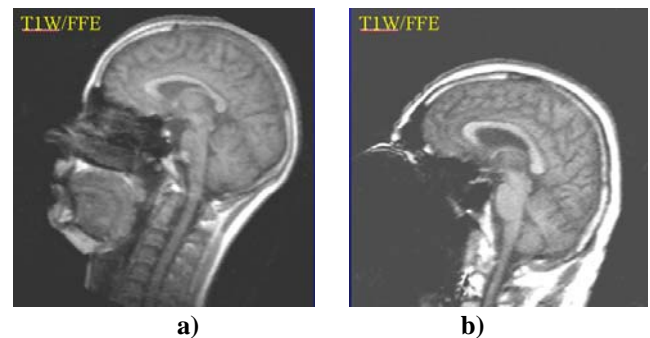*Karel BARTUSEK[1], Pavel FIALA[2], Jan MIKULKA[2]*

[1]Inst. of Scientific Instruments, Academy of Sciences of the Czech Republic, Královopolská 147, 612 00 Brno, Czech Rep.
[2] Dept. of Theoretical and Experimental Electrical Engineering , Faculty of Electrical Engineering and Communication, Brno University of Technology, Kolejní 2906/4, 612 00 Brno, Czech Republic

bar@isibrno.cz, fialap@feec.vutbr.cz, xmikul16@stud.feec.vutbr.cz

Abstract. *The possibility is studied of numerical modeling of magnetic field deformations in the environment of measured diamagnetic and paramagnetic samples for the purposes of studying magnetic resonance (MR) image deformations owing to the susceptibility of heterogeneous materials (objects). The verification was realized using a simple sample configuration (circular plate), and the numerically modeled cross-sections were compared with the experimentally obtained values of the magnetic field measured by the MR gradient echo technology. The results show that it is possible – via a technical calculation – to determine a magnetic field deformation in the environment of complex-shaped or non-homogeneous structures in the MR experiments.*

Keywords

Magnetic resonance (MR), numerical modeling, magnetic resonance imaging (MRI), magnetic field mapping, finite element method (FEM).

1. Introduction

Nuclear Magnetic Resonance (NMR) is a well-known non-destructive and non-invasive diagnostic method [1] - [5] that is used in investigations of materials properties. One of the fields that feature frequent uses of the NMR is the medical application. The magnetic resonance imaging (MRI) system can be used to propel the ferromagnetic nuclei [6]. This concept was studied for future development of micro-devices designed to perform minimally invasive interventions in remote sites accessible through the human cardiovascular system. A mathematical model is described in [6], taking into account various parameters like the size of blood vessels, the velocities and viscous properties of blood, the magnetic properties of materials, the characteristics of MRI gradient coils, or the ratio between the diameter of a spherical core and the diameter of the blood vessels.

The results of the NMR method and signal processing are material-sensitive, namely when the applied materials feature extreme differences in aspects like susceptibility, conductivity, and permeability from the macroscopic view of the matter. This leads to deformations and makes the NMR unusable; an example image in Fig. 1 shows the partial image loss effect.

Fig. 1. The two MRI results: the correct results a), the results with imaging loss.

There are two ways of enhancing the MR image resolution. The first one is oriented toward the enhancement of image processing [7] through the use of different means including numerical methods such as the FEM. This option is aimed at the geometry improvement and at the change of resulting images owing to different susceptibilities. The second way [8] is focused on the comparison of the measured sample with the numerical model; here, applying the numerical and the analytical techniques, the problem dealt with the effect of the sample and its susceptibility on the homogeneous magnetic field of tomograph system.

This paper describes the combined numerical - experimental inverse method, which can reduce the influence of materials with extreme differences on the properties; the basis of the applied approach lies in the semi-analytic method [8]. The inverse methods are used in different applications [5], [7], [9].

The idea of increase of the MRI quality is in the hybrid experimental and numerical inverse method. The numerical results are used in the MRI experimentally obtained data. The application of numerical results to the NMR post-processing can substantially increase the quality of the final images.

This paper describes the possibility of numerical modeling of magnetic field deformations in the environment of measured diamagnetic or paramagnetic samples for the purposes of studying MR image deformations owing to the susceptibility of heterogeneous materials (objects).

The verification of results was realized using a simple sample configuration (circular plate), and the numerically modeled cross-sections were compared with the experimental data obtained from the magnetic field measured by the MR gradient echo methods. The results show that it is possible – via a technical calculation – to determine the magnetic field deformation in the environment of complex-shaped or non-homogeneous structures in the MR experiments.

2. Magnetic Susceptibility Effect on the MR Image

Magnetic susceptibility of the measured sample or tissue affects the magnetic field both inside the sample and in its environment. As the resonance frequency of the nuclei depends on the induction of the magnetic field where the nuclei are located, the MR image deformations owing to the magnetic field deformations may occur.

There exist two basic MR measurement methods. In the spin-echo method, which is based on the excitation of nuclei applying two radiofrequency (RF) pulses as well as on the scanning of spin echo signals with the maximum in echo-time T_E (at this time, the magnetization vectors are in phase), there occurs the compensation of the effect of magnetic field non-homogeneity on the MR image. The received signal amplitude depends on the spin density, which is expressed by the magnetization vector $\boldsymbol{M}_0$.

$$\boldsymbol{M}_\perp\left(T_E\right) = \boldsymbol{M}_0 \left(1 - e^{-\frac{T_R}{T_1}}\right) e^{-\frac{T_E}{T_2}} \tag{1}$$

where T_1 and T_2 are relaxation times.

The gradient echo method (GE) [3] induces the defined dephasing of nuclei by the gradient magnetic field impulse and, then, the phase matching by a gradient impulse of the opposite polarity. The gradient echo forms in time T_E. In using this method there does not occur the compensation of non-homogeneity of the elementary magnetic field, and the final image contains artifacts induced by the local change of susceptibility in the measured sample excited volume. For further purposes we will introduce a reaction field with flux density $\Delta\boldsymbol{B}$ as an incremental field added to basic static magnetic field with flux density $\boldsymbol{B}_0$. The reaction field has flux density

$$\Delta\boldsymbol{B}\left(x,y,z\right) = \boldsymbol{B}\left(x,y,z\right) - \boldsymbol{B}_0 . \tag{2}$$

Noticeable reaction field variations can be observed on sharp edges of susceptibility changes in the measured sample. The magnetic field non-homogeneity induces the dephasing of the magnetization vectors of the sample nuclei.

The magnetization vector at time T_E will be

$$\boldsymbol{M}_\perp\left(T_E\right) = \boldsymbol{M}_0 \; e^{-\frac{T_E}{T_2^*}} e^{-\gamma\Delta B T_E} \tag{3}$$

where the exponential element e^{T_E/T_2^*} describes the magnetization decrease given by the dephasing of the magnetization vector of the nuclei owing to the effective relaxation time T_2^*, which is

$$\frac{1}{T_2^*} = \frac{1}{T_2} + \gamma\,\Delta\boldsymbol{B} \; , \tag{4}$$

and the element $e^{-\mathrm{j}\cdot\gamma\Delta B T_E}$ expresses the MR image phase modulation induced by $\Delta\boldsymbol{B}$. By evaluating the signal obtained via the GE method we get the MR image, in whose phase

$$\Delta\psi = \gamma\Delta B T_E , \tag{5}$$

the spatial distribution of the sample reaction magnetic field is encoded. If the reaction field $\Delta\boldsymbol{B}$ is induced by the magnetic susceptibility of the sample, then, depending on a suitable arrangement of the experiment, it is possible to evaluate the magnitude of magnetic susceptibility of an unknown material.

The reaction field size can be as large as to shorten the effective relaxation time T_2^* to a size smaller than that of the sampling period for the signal scanning. On this condition, both the SE and GE methods will show, at the point of an increased reaction field value, a decrease in the signal amplitude as well as a module size decrease in the MR image [1]. On these conditions, there occur a local signal loss and the MR image deformation. From equation (1), when using the GE sequence, we need to work with the short echo time T_E.

3. Numerical Modeling

3.1 The Numerical Model

In measuring the susceptibility of material samples, the complex configurations of the NMR measuring equipment do not always provide unambiguous output values. Therefore, it is necessary to find a technique of reliable verification of measured results. One of the alternatives consists in modeling the given configuration numerically using the FEM together with the Ansys system. Significantly, Ansys is suitable for multiphysical processes, anisotropic materials, and offers the option of using the special APDL programming language. These advantages have not yet been joined together by any other program. More information can be found in references [8] and [11]. We solve the system of equations:

$$\left[k_{ij} \right] \cdot \left[\varphi_i \right]^{\mathrm{T}} = 0 , \ i,j \in \{1,\dots NN\} , \tag{6}$$

which can be arranged to the form

$$\mathbf{K} \begin{bmatrix} \mathbf{U}_{\mathrm{I}} \\ \mathbf{U}_{\mathrm{D}} \end{bmatrix} = \begin{bmatrix} 0 \\ 0 \end{bmatrix} \tag{7}$$

where $\mathbf{U}_{\mathrm{I}} = [\varphi_1,\dots,\varphi_{NI}]^{\mathrm{T}}$ is the vector of unknown potentials of internal nodes belonging to the area Ω including the points along the boundaries Γ_3 and Γ_4 (the Neumann boundary conditions). $\mathbf{U}_{\mathrm{D}} = [\varphi_1,\dots,\varphi_{ND}]^{\mathrm{T}}$ is the vector of known potentials at the boundaries Γ_1 and Γ_2 (the Dirichlet boundary conditions). NI in the index marks the number of internal nodes of the discretization mesh; ND is the number of the mesh boundary nodes.

The system of equations (6) can be solved by standard algorithms. The scalar magnetic potential value is then used for evaluating the magnetic field.

3.2 The Geometrical Model of an Isolated Non-homogeneity

The geometry of the task for numerical modeling is depicted in Fig. 2. The examined material sample is an isolated (glass) ball filled with water and surrounded by clay along all sides. In total, the model includes four different volumes with different susceptibilities: material no. 4 – outer medium (air), $\chi_4=0$, material no. 3 – clay, $\chi_3=-8.85\cdot10^{-6}$, material no. 2 – glass, $\chi_2=-11.67\cdot10^{-6}$, material no. 1 – non-homogeneity – water $\chi_1=-12.44\cdot10^{-6}$. The materials are defined by their permeabilities using the relation $\mu=1+\chi$.

The geometrical model according to Fig. 2 was built using the FEM and applying the Solid96 mesh of elements in the Ansys system [12]. The boundary conditions were selected for the magnetic flux density value of the static elementary field to be $B_0=4.7$ T in the direction of the coordinate z (in cube axis), which corresponds with the real experiment carried out using the MR tomograph at the Institute of Scientific Instruments, Academy of Sciences of the CR in Brno. In Fig. 2 the path is shown along which there were displayed the material cross-section results for the distribution of the magnetic flux density B module in Figs. 3–5.

Consequently, for the scalar magnetic potential φ_{m} there holds

$$\boldsymbol{H} = -\mathrm{grad}\,\varphi_{\mathrm{m}} . \tag{8}$$

The potential of the exciting static field $\boldsymbol{H}_0$ is after applying the Neumann boundary conditions:

$$\varphi_{\mathrm{m}} = \int \boldsymbol{H}_0 \cdot \boldsymbol{u}_z \mathrm{d}z = H_0 \cdot z \tag{9}$$

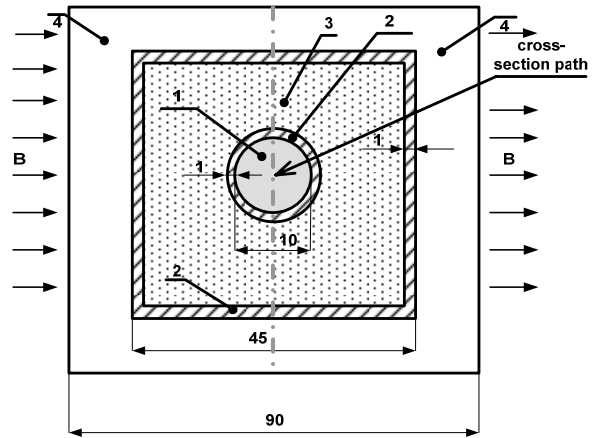where $H_0 = \dfrac{B_0}{\mu_0 \cdot \mu_r}$. \hfill (10)

Fig. 2. Geometry for numerical modeling, sizes in mm.

By applying (9) the Dirichlet boundary condition it can be computed for this model

$$\pm \frac{\varphi_{\mathrm{m}}}{2} = \frac{B_0 \cdot z}{2\mu_0} = \frac{4.7 \cdot 90 \cdot 10^{-3}}{2\mu_0} \tag{11}$$

where z is the total length of the model edge. For the model meshing, the element size selected as optimum was $0.125\cdot10^{-3}$ m. The boundary conditions $\pm \varphi_{\mathrm{m}}/2$ were set on the model external left and right boundaries, as is shown in Fig. 2. This is derived for the assumption that, in the entire area, there are no exciting currents, therefore there holds for the curl$\boldsymbol{H}=0$ and the field is irrotational.

Using the Ansys system, we obtained the maps of B distribution. The cross-sections of these maps are in Fig. 3 - the result for the model Fig. 2 with water in the ball, and in Fig. 4 - the model with clay in this ball (homogeneous material) as a background. The influence of dissimilar susceptibility of the wall material is noticeable.
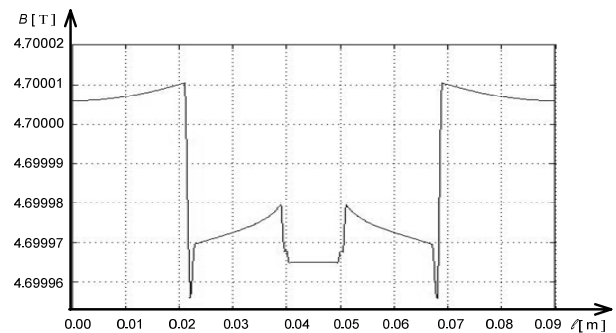

Fig. 3. Distribution of the module of magnetic flux density B for the non-homogeneity with water, $\chi_1=-12.44\cdot10^{-6}$, ANSYS analysis results.

Now, the differential image can be obtained by subtracting Fig. 4 from Fig. 3, see Fig. 5. For the isolated non-homogeneity according to Fig. 2, the value of the change of magnetic flux density module can be read from Fig. 5 and is equal to $\Delta B = 14.76 \ \mu\mathrm{T}$.
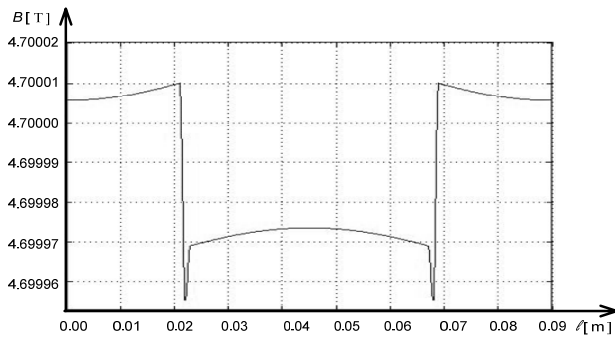
Fig. 4. Distribution of the module of magnetic flux density B for the clay background, $\chi_3 = -8.85 \cdot 10^{-6}$, ANSYS analysis results.
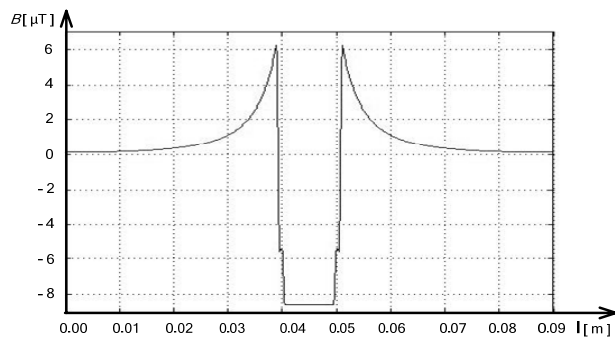

Fig. 5. Distribution of the module of magnetic flux density B for the non-homogeneity with water after subtracting the clay background, $\Delta B = 14.76\ \mu T$, ANSYS numerical analysis results.

4. Experimental Verification of the Isolated Non-homogeneity Model

The results of the numerical analysis were experimentally verified using the 200 MHz/75 mm MR tomograph at the Academy of Sciences of the Czech Republic. The tomograph basic magnetic field $B_0 = 4.7$ T is generated by a superconducting horizontal magnet produced by Magnex Scientific Company.

The reference sample was a square section vessel filled with clay ($\chi = -8.85 \cdot 10^{-6}$). The vessel held a water-filled ($\chi = -12.44 \cdot 10^{-6}$) glass ball with the diameter of 10 mm. In order to accelerate the measuring process, the relaxation time T_2 of water was shortened by adding 1 mol of nickel sulphate $NiSO_4$ and sodium chloride $NaCl$. The relaxation time of water was $T_2 \approx 175$ ms. The rectangular layout of the cross-section (Fig. 7) corresponds to the geometry in Fig. 2 and has been selected to facilitate an easier evaluation of the field flux density course.

In Fig. 8 the measured MR spectrum of the isolated non-homogeneity from Fig. 2 is shown. All ^{1}H nuclei surrounded by clay are measured. The clay represents the agent changing the magnetic field in the water and, therefore, there occurs the resonance line shift of $\Delta f = 657$ Hz. This shift corresponds with the change of the magnetic field of

$$\Delta B = \frac{2\pi\, \Delta f}{\gamma} = \frac{2\pi\, \Delta f}{2.67 \cdot 10^8} = 15.44\ \mu T\,, \qquad (12)$$

where γ is the gyromagnetic ratio of ^{1}H nuclei in water. This is in good agreement with $\Delta B = 14.76\ \mu T$ obtained from the numerical modeling (Fig. 5).
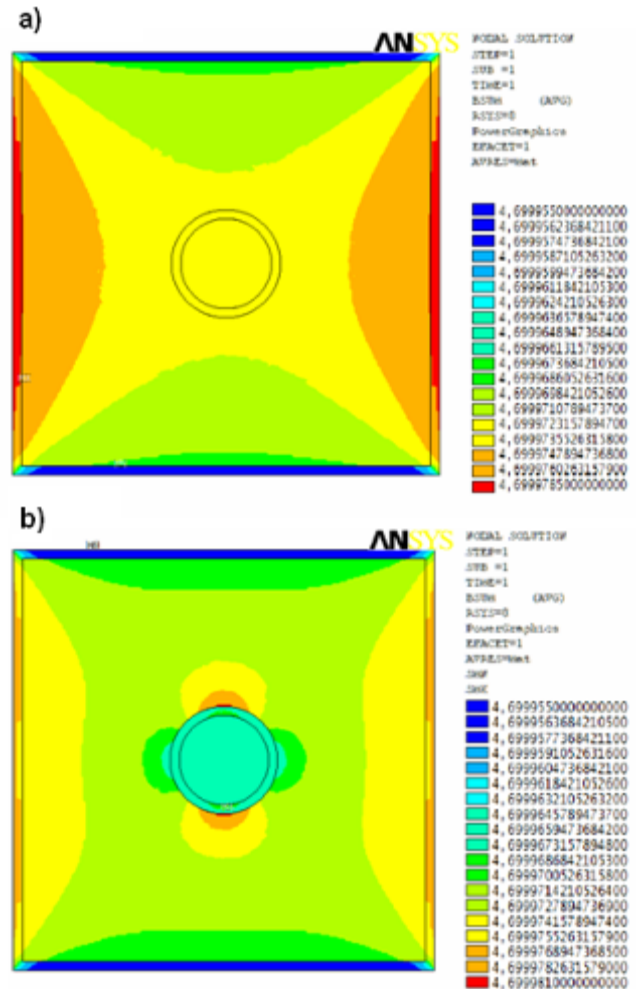

Fig. 6. The FEM numerical analysis in the ANSYS system, the distribution of the magnetic flux density B module (T), a) clay in a glass cube, without non-homogeneity with water, b) clay in a glass cube, non-homogeneity with water inside.


Fig. 7. A view of the measuring vessel with the 10 mm diameter glass ball inside without filled clay.

The spectral line half-width is 400 Hz, which corresponds with the maximum magnetic field change $\Delta B = 9.4$ µT.
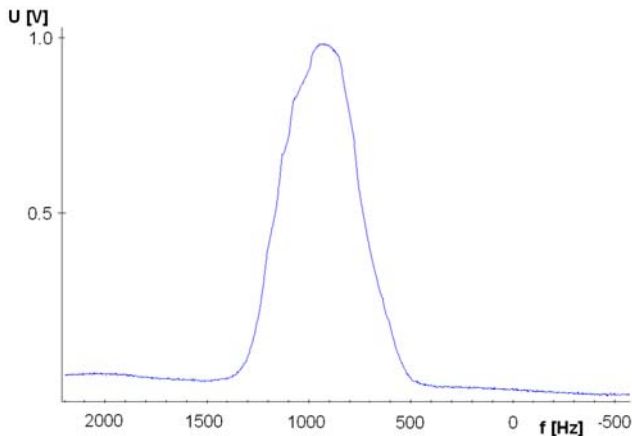
Fig. 8. Measured spectral characteristics of MR signal of an isolated non-homogeneity, frequency shift $\Delta f = 657$ Hz. (measured resonance frequency offset without the clay is 155 Hz).

Magnetic field distribution in the cross-section of the sphere centre can be obtained from the MR image scanned using the GE method. The data obtained by applying this method feature the encoded change of magnetic field flux density, see (5). Fig. 9 shows the MR phase picture measured by the GE method with $T_E = 5$ ms for the spherical sample with the diameter of 10 mm surrounded by clay. The maximum magnetic field change inside the sphere is 7.7 µT and the corresponding spectral line half-width is 330 Hz.
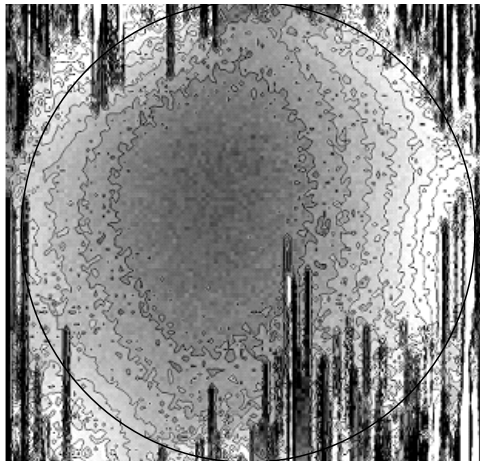
Fig. 9. The map of magnetic field induction in a plane perpendicular to the elementary field and running through the centre of a sphere (10 mm diameter). The equipotentials are to $B = 1$µT.

The numerical modeling and task analysis in the isolated non-homogeneity confirmed the experimental results and, thanks to the modifiability of the numerical model, we succeeded in preparing simulation experiments to analyze the magnetic field deformations in porous materials and to enhance the accuracy of measuring magnetic susceptibility in materials that do not form the MR signal by the help of the MR method.

5. Conclusion

Applying the numerical analysis method, we calculated the isolated inhomogeneity magnetic field maps induced by the magnetic susceptibility of material in selected arrangements. The obtained results were compared with the experimental measuring results of corresponding configurations performed using the MR tomograph.

The spectral line frequency shift of 657 Hz corresponds to the magnetic field variation of 15.44 µT. The calculated shift of 14.76 µT agrees well with the experimental measurement. The magnetic susceptibility of clay depends considerably on its composition, and the susceptibility value range is wide. For the selected model corresponding to the experiment, the iteratively established magnitude of the magnetic susceptibility of clay was $\chi = -8.85 \cdot 10^{-6}$. The magnetic susceptibility of the applied sample of clay measured using the NMR method [8] is $\chi = -8.7 \cdot 10^{-6}$, which forms a very good agreement with the numerical modeling results. For the water-filled cavity in clay, the map of magnetic field induction was measured. The maximum variation of magnetic induction is 7.7 µT, and this value is consistent with the value determined from the spectral line half-width. The MR spectra and magnetic field map were measured applying the MR gradient echo method with good agreement with the calculated results.

The proposed procedure joins together the numerical modeling of magnetic field distribution in the measured samples investigated using the NMR techniques; the results are compared with the NMR experiment. The same model will be used for the inverse task. The measured map of magnetic induction in the sample zones with different magnetic susceptibility will be iteratively modeled and the magnitudes will be determined of magnetic susceptibility in the individual zones. This hybrid procedure is very interesting and will be utilized for the numerical modeling of porous materials and the behavior of liquids and gases in the pores.

The numerical models are designed for inversion tasks of magnetic field deformations simulation in measurement using the MR tomograph and, further, for evaluating the magnetic susceptibility measurement using MR methods in samples that do not form the MR signal.

Acknowledgements

References

[1] VLAARDINGERBROEK, M. T..; DEN BOER, J. A. *Magnetic Resonance Imaging*. Heidelberg (Germany): Springer-Verlag, 1999, ISBN 3-540-64877-1.

[2] SLICHTER, C. P. *Principles of Magnetic Resonance*. Second revised and expanded edition, corrected second printing. Berlin (Germany): Springer-Verlag, 1980.

[3] HAACKE, E. M.; BROWN, R. W.; THOMPSON, M. R.; VENKATESAN, R. *Magnetic Resonance Imaging – Physical Principles and Sequence Design*. John Wiley & Sons, 2001, ISBN 0-471-48921-2.

[4] ARIMA, H. K.; MAEHATA S.; ISHIBASHI, K.; NAKAMOTO, T.; SHINTOMI, T. Multipole analysis for absolute magnetic field measured by multi-probe pulsed-NMR method. *IEEE Transactions on Applied Superconductivity*, March 2000, vol. 10, no. 1, pp. 1450 - 1453, ISSN 1051-8223.

[5] ZHANG, Z. Q., LIU, Q. H. Two nonlinear inverse methods for electromagnetic induction measurements. *IEEE Transactions on Geoscience and Remote Sensing*, June 2001, vol. 39 , no. 6, pp. 1331 to 1339, ISSN 0196-2892.

[6] MATHIEU, J.-B., BEAUDOIN, G., MARTEL, S. Method of propulsion of a ferromagnetic core in the cardiovascular system through magnetic gradients generated by an MRI system. *IEEE Transactions on Biomedical Engineering*, Feb. 2006, vol. 53, no. 2, pp. 292 - 299, ISSN 0018-9294.

[7] SUMANAWEERA, T. S., GLOVER, G. H., BINFORD, T. O., ADLER, J. R. MR susceptibility misregistration correction. I*EEE Transactions on Medical Imaging*, June 1993, vol. 12, no. 2, pp. 251–259, ISSN 0278-0062.

[8] STEINBAUER, M., KROUTILOVÁ, E. Measurement of weakly magnetic material using new MR technique. In *Proceedings of Applied Electronics 2006*. Pilsen (Czech Republic), 2006. pp. 87-91, ISBN 80-7043-442-2.

[9] FIALA, P., KROUTILOVÁ, E., STEINBAUER, M., HADINEC, M., BARTUŠEK, K. Inversion reconstruction of signals measured by the NMR techniques. In *Proceedings of PIERS 2007*. Prague (Czech Republic), pp. 363-366, ISSN 1559-9450.

[10] REULET, P., NORTERSHAUSER, D., MILLAN, P. Inverse method using infrared thermography for surface temperature and heat flux measurements. In *Proceedings of 20th International Congress on Instrumentation in Aerospace Simulation Facilities*. Gottingen (Germany), 25-29 Aug. 2003, pp. 118 - 126. ISBN 0-7803-8149-1.

[11] BARTUŠEK, K., DOKOUPIL, Z. Magnetic resonance diffusion measurement method in heterogenous systems. In *Modern Development of Magnetic Resonance 2007*. Kazan (Russian Federation): Zavoisky Physical Technical Institute Kazan, 2007. pp. 142-143.

[12] Houston (USA): Ansys User's Manual. Svason Analysys System, Inc., Houston, USA, 1994-2006.

About Authors...

Karel BARTUSEK was born in Brno, Czech Republic, in 1949. He received the Ing. (MSc.) degree in Electrical Enginnering in 1973, the CSc. (PhD.) degree in 1983, DrSc. Degree in 1998 and Prof. degree in 2008. He works as an independent scientific worker at the Institute of Scientific Instruments in Brno, Academy of Sciences of the Czech Republic and as a scientific worker at the Brno University of Technology, Faculty of Electrical Engineering and Communication.

Pavel FIALA received Ph.D. in Electrical Engineering from the Brno University of Technology, Faculty of Electrical Engineering and Communication in 1998. He joined the Department of Theoretical and Experimental Electrical Engineering in 1990 as a research assistant. Since 2003 he has been an Associate professor and head of the Department of Theoretical and Experimental Electrical Engineering. Dr. Fiala is interested in modeling and analysis of coupled problems by numerical method formulated with partial differential equations using the finite element method (FEM), the boundary element method, the finite difference method.

Jan MIKULKA received his Ing. (MSc) degree in Electrical Engineering from the Brno University of Technology in 2007. He is a PhD student at the Dept. of Theoretical and Experimental Electrical Engineering. His research work is concerned on problems aimed at NMR imaging, segmentation, especially image segmentation.